ELSEVIER

Fluid Dynamics Research 19 (1997) 343–362

FLUID DYNAMICS RESEARCH

Görtler vortices promoted by wall roughness

Alessandro Bottaro[a,*], Abdelfattah Zebib[b]

[a] *IMHEF-DGM, Ecole Polytechnique Fédérale de Lausanne, CH-1015 Lausanne, Switzerland*
[b] *Department of Mechanical and Aerospace Engineering, Rutgers University, New Brunswick, NJ 08903, USA*

Received 9 April 1996; accepted 26 June 1996

Abstract

Numerical experiments are conducted to investigate spatially developing Görtler vortices and the way in which wall roughness promotes their formation and growth. Several different types of walls are examined and their relative merits as vortex promoters assessed. The only disturbances of the flow are due to the rough wall; hence, at each downstream station the local field feels (1) the upstream flow distribution (produced by the upstream wall conditions) and (2) the local forcing at the wall. Rapid vortex formation and growth, like in the case of ribleted walls, can be qualitatively explained by the positive combination of these two effects; when the two influences on the local flow field compete, e.g. for randomly distributed wall roughness, the equations with the boundary conditions filter the disturbances over some streamwise length, *function of the roughness amplitude*, to create coherent patches of vorticity out of the random noise. These patches can then be amplified by the instability mechanism. If a thin rough strip is aligned along the span of an otherwise smooth wall to trip the boundary layer, the filtering region is shorter and growth of the vortices starts earlier. Also for the case of an isolated three-dimensional hump a rapid disturbance amplification is produced, but in this case the vortices remain confined and a very slow spanwise spreading of the perturbation occurs. In all naturally developing cases, where no specific wavelengths are explicitly favored, the average spanwise wavelengths computed are very close to those of largest growth from the linear stability theory.

1. Introduction

In all problems of linear stability (e.g. the Görtler problem) a small perturbation is needed so that a stable solution (the two-dimensional boundary layer flow) can bifurcate and a new stable state (with steady streamwise-oriented vortices) ensues. The small perturbation is the "seed" required to initiate the vortex formation; it acts at the boundaries of the physical domain and may take several forms such as inlet inhomogeneities (e.g. honeycomb grids), free-stream turbulence and acoustic disturbances, distributed or isolated wall roughness elements. In any experimental set up it is typically a combination of several of these effects which is responsible for the instability of the base flow. This multiplicity of causes is the reason why experimental results for Görtler vortices

* Corresponding author.

PII S0169-5983(96)00055-X

differ widely from one apparatus to another (compare e.g. wavelength results from Tani [1], Bippes and Görtler [2] and Swearingen and Blackwelder [3]) and are sometime not even reproducible on the same apparatus [4]. Matters are further complicated by the fact that a very large range of wave numbers exists with almost equal spatial amplification rate [5, 6]: the wavelength selection mechanism is very weak.

Theoretical/numerical studies have the advantage over experimental work to permit a clear definition of the boundary effects and to allow their complete isolation. It becomes then possible to determine if one cause is preponderant in promoting the vortex development and if so why. Our current understanding of the Görtler instability suggests that the leading sources of stationary streamwise vorticity are upstream screens (i.e. initial spatial conditions) and wall roughness. The former vortex "seed" has been studied by Hall [7] with a linear theory and by Bottaro et al. [6] with non-linear simulations: Bottaro et al. found a linear response of the vortices with increasing screen-induced perturbations, up to very large initial disturbance amplitudes. The latter "seed" of vortex formation is the object of the present work. Its importance in practical applications stems from the fact that, e.g. on wing surfaces, imperfections due to manufacturing processes, corrosion, surface stresses, icing or even insect impingement, are known to affect transition location in a wide variety of flow situations.

The literature on the receptivity of Görtler vortices to roughness is rather scarce. Denier et al. [8] considered a wall with different streamwise and spanwise roughness scales. The small and the O(1) wavelength limits were examined with linear theory. Their O(1) results were later extended and corrected by Bassom and Hall [9], who indicated that distributed roughness is a very efficient mean of vortex generation: the critical Görtler number becomes arbitrarily small, the closer the wall forcing is applied to the plate's leading edge. Furthermore, they predicted that in the absence of distributed roughness, isolated roughness elements would have a prevailing role in triggering vortices only in an environment virtually free of free-stream disturbances. Bertolotti [10] solved by a linear parabolized streamwise marching technique (the PSE approach) the equations for the flow over concave surfaces with streamwise aligned wall corrugations. This riblet-like wall was found to be very conducive to the formation and development of vortices, even for riblets' wavelength different from that of the inlet vortex. Bertolotti also found that vortices are receptive to the wall forcing over an extended streamwise distance.

The first experimental verification that the Görtler vortex wave number depends on the nature of the incoming perturbation field was provided by Bippes and Görtler [2]. Swearingen and Blackwelder [11] confirmed this upstream influence by introducing strips of tape at the wall and by positioning cylinders in the incoming flow, with the aim of isolating the wavelength selection mechanism. The upstream influence clearly arises from the parabolic nature of the governing disturbance equations for O(1) wavenumbers [12]. Recent experiments by Bippes and Deyhle [13] indicate that the Görtler instability in a wind tunnel is primarily promoted by the screens in the settling chamber.

The situation is somewhat different in three-dimensional boundary layers, such as those over swept wings. In a low-disturbance environment it has been experimentally demonstrated [14–16] that stationary cross-flow vortices are preferentially excited and the location of their appearance is intimately tied to micron-sized roughness in the model; this correlation was investigated by Radeztsky et al. [17] who found an increase in the transition Reynolds number with subsequent levels of polishing of the wall. Radeztsky et al. also placed isolated roughness elements on their swept surface to find a dependence of the transition "point" on roughness location, dimensions and spanwise spacing of the elements. Stationary cross-flow vortices are profoundly affected by the presence of roughness

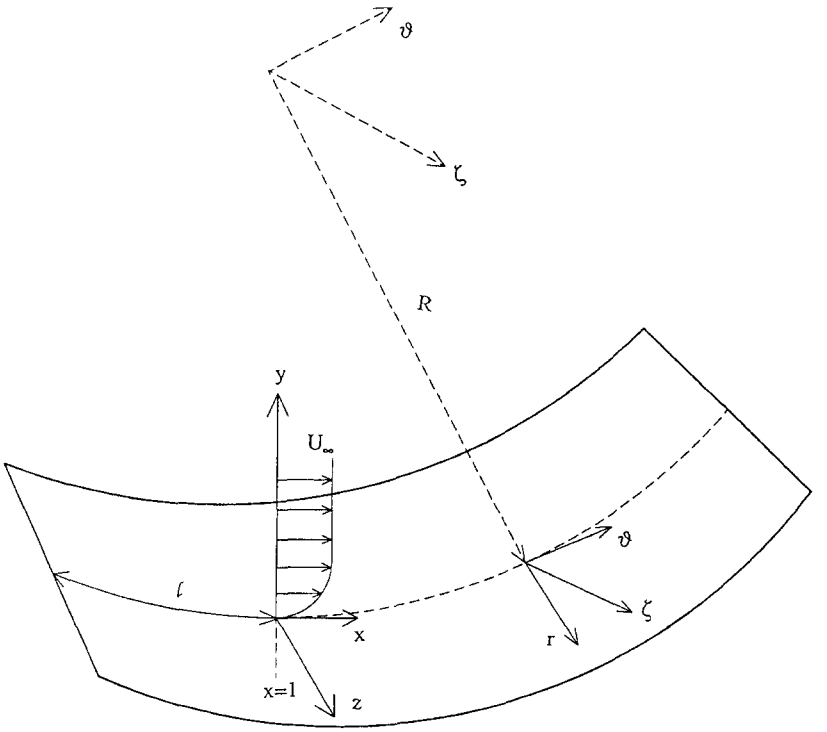

Fig. 1. Sketch of the problem.

close to the plate's leading edge [18]. On the other hand, it appears that sound has no significant effect on this type of transition [19].

In the present study different rough surfaces are examined and compared for their effect on triggering the initial vortex: The perturbation to the base flow is provided by the fact that the wall is not smooth, and hence a small distance from the wall an inhomogeneous velocity distribution is produced. It will be shown that minute wall imperfections are sufficient to destabilize the basic flow and that riblet-like surfaces are most conducive to the downstream formation of stationary Görtler vortices.

2. Physical configuration, equations and boundary conditions

The physical configuration considered is sketched in Fig. 1. Fluid flows over a concave surface of large streamwise and spanwise extents. A boundary layer is formed at the wall and, in the limit of large Reynolds number and radius of curvature, it is governed by the Prandtl equations.

The boundary layer flow over a concave wall with constant radius of curvature R has been described by several authors (see, for instance, Ref. [12]). The starting point of the analysis is the system of Navier–Stokes and continuity equations in cylindrical coordinates (r, θ, ζ); l is taken to be a typical length along the wall and a curvature parameter κ, a Reynolds number Re and a Görtler

number G are introduced:

$$\kappa = lR^{-1}, \quad \mathrm{Re} = U_\infty l/\nu, \quad \mathrm{G}^2 = \kappa\,\mathrm{Re}^{1/2}, \tag{1}$$

with U_∞ the free stream velocity and ν the kinematic viscosity. The limits $\kappa \to 0$ and $\mathrm{Re} \to \infty$ are taken such that $\mathrm{G} = \mathrm{O}(1)$. We define the dimensionless boundary layer coordinates x, y, and z through:

$$x = \frac{\theta}{\kappa}, \quad y = [(-r - R)/l]\mathrm{Re}^{1/2}, \quad z = (\zeta/l)\mathrm{Re}^{1/2}. \tag{2}$$

and the dimensionless velocities u, v, w and pressure p:

$$u = \frac{v_\theta}{U_\infty}, \quad v = -\frac{v_r}{U_\infty}\mathrm{Re}^{1/2}, \quad w = \frac{v_\zeta}{U_\infty}\mathrm{Re}^{1/2}, \quad p = \frac{p'}{\rho U_\infty^2}\mathrm{Re}, \tag{3}$$

where ρ is the density and p' is the dimensional pressure. When these variables are introduced into the Navier–Stokes equations, the leading order system is found:

$$\frac{\partial u}{\partial x} + \frac{\partial v}{\partial y} + \frac{\partial w}{\partial z} = 0, \tag{4}$$

$$\left[u\frac{\partial}{\partial x} + v\frac{\partial}{\partial y} + w\frac{\partial}{\partial z}\right] u = \frac{\partial^2 u}{\partial y^2} + \frac{\partial^2 u}{\partial z^2}, \tag{5}$$

$$\left[u\frac{\partial}{\partial x} + v\frac{\partial}{\partial y} + w\frac{\partial}{\partial z}\right] v + G^2 u^2 = -\frac{\partial p}{\partial y} + \frac{\partial^2 v}{\partial y^2} + \frac{\partial^2 v}{\partial z^2}, \tag{6}$$

$$\left[u\frac{\partial}{\partial x} + v\frac{\partial}{\partial y} + w\frac{\partial}{\partial z}\right] w = -\frac{\partial p}{\partial z} + \frac{\partial^2 w}{\partial y^2} + \frac{\partial^2 w}{\partial z^2}, \tag{7}$$

These equations are parabolic and can be marched from an initial streamwise position $x = 1$. The terms neglected are formally of order Re^{-1}. Notice that time is ignored because of experimental evidence [1–3] in the early development. An a posteriori justification for employing the parabolic model (4)–(7) in the present study is given in Appendix.

At the inflow of the computational domain only the Blasius velocity distribution is imposed. At the free-stream zero y-derivatives of the three velocity components are specified, and at the lateral edges symmetric conditions are applied. Only wall roughness, simulated with the adoption of non-zero slip velocities at $y = 0$, can act as a trigger for the vortices. If the "true" wall is represented by $y = \varepsilon g(x, z)$ we have:

$$u = v = w = 0 \quad \text{at } y = \varepsilon g(x, z), \tag{8}$$

with ε the roughness amplitude and $g(x, z)$ the roughness distribution function. For small roughness amplitude we can Taylor expand Eq. (8) as

$$u(x, \varepsilon g, z) = u(x, 0, z) + \left.\frac{\partial u}{\partial y}\right|_{y=0} \varepsilon g(x, z) + \mathrm{O}(\varepsilon^2), \tag{9}$$

and similarly for v and w. The computational domain in the vertical direction extends from $y = 0$, where the Robin-type boundary condition

$$u(x,0,z) + \left.\frac{\partial u}{\partial y}\right|_{y=0} \varepsilon g(x,z) = 0 \tag{10}$$

is implicitly enforced (and likewise for the other two components). Other authors (i.e. Ref. [20]) have used the same conditions to simulate rough walls. The boundary conditions are accurate up to $O(\varepsilon)$: the smallest order terms retained in Eq. (10) must be larger than the terms neglected in Eqs. (4)–(7). This leads to

$$\varepsilon \gg \mathrm{Re}^{-1}. \tag{11}$$

Furthermore, for first-order boundary layer theory to be applicable and to avoid the appearance of macroscopic recirculating flow zones the inequalities

$$\varepsilon \leqslant \Delta y_{\min} \ll 1 \tag{12}$$

should hold, with $\Delta y_{\min}$ the minimum grid distance along the vertical direction. Such a minimum grid length is that of the control surface adjacent to the wall for the non-uniform mesh employed in the present calculations. With requirements (11) and (12) on ε, the (parabolic) boundary layer equations are appropriate to describe the phenomenon under consideration (see also Refs. [7–10]); for larger roughness amplitudes other models must be used to capture eventual regions of backflow.

Taking as a basis the experiments of Swearingen and Blackwelder [3] we can obtain some typical roughness amplitudes. For a flow of air ($\nu = 0.15\,\mathrm{cm}^2/\mathrm{s}$) with $U_\infty = 500\,\mathrm{cm/s}$, it is $\mathrm{Re}^{-1} = 7.5 \times 10^{-6}$ when l is 40 cm. One can therefore perform numerical experiments with roughness amplitudes ranging from, for example, 0.003 (corresponding to 3 μm) to 0.05 (55 μm): these are realistic measures that allow appreciation of the impact of surface finish.

3. Numerical solution technique and governing parameters

The numerical approach is the same as that used by Bottaro et al. [6] in a recent study of spanwise rotating Görtler vortices. Only the main features of the technique are given here. The flow cross-section is subdivided into a finite number of non-overlapping control surfaces; second-order schemes are used in y–z to discretize convective and diffusive fluxes, and a fully implicit Euler scheme is used to march the equations downstream. The pressure is treated with a pressure correction algorithm (see Ref. [21]). 71 smoothly stretched control surfaces are employed to cover the y range[1] which spans from 0 to $y_e = 50$ and 151 regularly distributed control surfaces cover the z range which goes from 0 to $L = 89.7$; the streamwise marching step is taken equal to 0.02. The suitability of this mesh has been proven by comparisons with calculations on both coarser and finer grids and is fully documented in Ref. [6]. Note that the large dimension along the span has been chosen to allow the natural development of several neighboring vortex pairs: this way the wavelength of the instability

[1] The value of $\Delta y_{\min}$ is 0.0894.

is a result of the calculations, rather than being forced. One dimensionless measure of the spanwise wavelength which is frequently used is Λ, defined by

$$\Lambda = \frac{U_\infty \lambda'}{\nu}\sqrt{\frac{\lambda'}{R}}. \tag{13}$$

Λ remains constant at all streamwise locations (unless merging and/or splitting of vortices takes place and the physical wavelength λ' of the vortices is modified). Both local [5] and non-local [6] linear stability theories predict that the wavelength of maximum amplification is about $\Lambda = 210$ sufficiently downstream of the plate's leading edge.

All computations presented here start from $x = 1$ with $G = 6.756$; in Swearingen and Blackwelder's [3] parameter space this corresponds to $l = 40$ cm and $\mathrm{Re} = 133\,333$. The simulations are carried out through a filtering phase (where the flow receptivity operates), the linear growth phase and up to the early stages of non-linear saturation. Each calculation required of the order of 25 h of CPU time on the Cray Y-MP of the EPFL.

4. Types of walls considered and discussion of the results

Several kinds of surfaces have been considered by appropriately choosing the function $g(x, z)$ and, to facilitate comparisons, all the cases treated have been listed in Table 1. The influence of roughness amplitude can be inferred by comparison of cases 1 and 2 for a rough surface with stochastic distribution; the function $f_0(x, z)$ of Table 1 is made up of random numbers between -1 and 1. Cases 3–5 correspond to spanwise aligned rough strips, while case 6 is for walls with triangular grooves along the longitudinal direction (riblets) and 7 is the case of an isolated three-dimensional hump on a smooth wall.

To monitor the vortex formation and growth we focus on the streamwise disturbance energy $E = E(x)$, defined through

$$E = \int_0^L \int_0^{y_e} u_1^2 \, \mathrm{d}y \, \mathrm{d}z, \tag{14}$$

where u_1 is the deviation from the Blasius similarity solution. Other measures of the perturbation field have also been examined (energy of the local deviation from the spanwise averaged flow, for example) which have no effect on the conclusions reached.

Finally, the growth rate σ of the instability can be introduced as

$$\sigma = \frac{1}{2E}\frac{\mathrm{d}E}{\mathrm{d}x}. \tag{15}$$

4.1. Cases 1 and 2: Distributed wall roughness

When a broad band of roughness wavelengths is imposed – the common situation in most practical applications – Görtler vortices can start growing after an initial phase in which the equations and the boundary conditions filter the disturbances (Fig. 2, left). The length, in the streamwise direction, of

Table 1
Summary of the cases investigated

Case no.	ε	$g(x,z)$	Remarks
1	0.005	$f_0(x,z)$	*Random roughness.* Randomly distributed wall inhomogeneities can act as a vortex promoter mechanism. Larger amplitude roughness produces a more rapid vortex growth. The receptivity mechanism is linear. Average wavelength Λ close to 210.
2	0.025	$f_0(x,z)$ ($f_0(x,z)$: white noise distribution of amplitude in the interval $[-1,1]$)	
3	0.05	$f_1(x,z)\exp[-50(x-1.25)^2]$	*Rough Gaussian strip along z.* A rough Gaussian strip aligned along z is more efficient than distributed roughness. The vortex seeding is absent for spanwise aligned 2D roughness (case 4), while streamwise aligned 2D roughness (case 5) is very conducive to vortex formation. Average wavelength Λ close to 210.
4	0.05	$f_2(x)\exp[-50(x-1.25)^2]$	
5	0.05	$f_3(z)\exp[-50(x-1.25)^2]$ (f_1, f_2, f_3: white noise distributions of amplitude in the interval $[0,1]$)	
6	0.05	$\begin{cases} \frac{2}{s}(z-ks) \\ 2\left(1-\frac{z-ks}{s}\right) \end{cases}$	for $ks \leqslant z \leqslant (2k+1)s/2$, for $(2k+1)s/2 \leqslant z \leqslant (k+1)s$, $k = 0,1,2,\ldots$
6.1		$s = 3.588$	*Triangular riblets.* Each distribution prescribes a unique wavelength. Riblets are the best vortex promoter. Görtler vortices adjust to the riblets and acquire their wavelength. The faster growth is found for spanwise wavelength Λ of about 210. For $\Lambda < 50$ the vortices decay.
6.2		$s = 9.966$	
6.3		$s = 22.425$ (s: spanwise period of the riblets)	
7	0.05	$\exp[-50(x-1.25)^2]\exp[-(z-35)^2]$	The three-dimensional hump. It induces localized vortices with $\Lambda \approx 210$.

this phase increases with decreasing roughness amplitude, for fixed roughness distribution. This can be clearly inferred by inspection of the curves of growth rate σ with x (Fig. 2, center and right): a backward extrapolation towards $\sigma = 0$ indicates the "point" from which the perturbation starts growing for each case. It will be shown later that vortices of different amplification levels coexist at each x; hence, a unique point from which quasi-exponential growth begins does not really exist. However, it is clear that vortices are amplified earlier, on the average, for case 2 (with $\varepsilon = 0.025$) than for case 1 ($\varepsilon = 0.005$); i.e., *the length of the receptivity region depends on the roughness amplitude.* Unlike the case of random inflow perturbations (which mimics the situation of upstream grids) on a smooth wall, treated by Bottaro et al. [6], the disturbance energy does not decrease with x during the receptivity phase because the source of the perturbation – the rough wall – is active over an extended streamwise distance.

During the initial phase coherent patches of alternating positive and negative streamwise vorticity of "appropriate" dimensions are formed near the wall. In Fig. 3 cross-sections at $x = 1.1 + 0.2i$, $i = 0,1,\ldots,9$, of positive (light shading) and negative (dark shading) streamwise vorticity are shown for case 1. Initially, large-scale regions of very weak positive and negative vorticity are formed. With

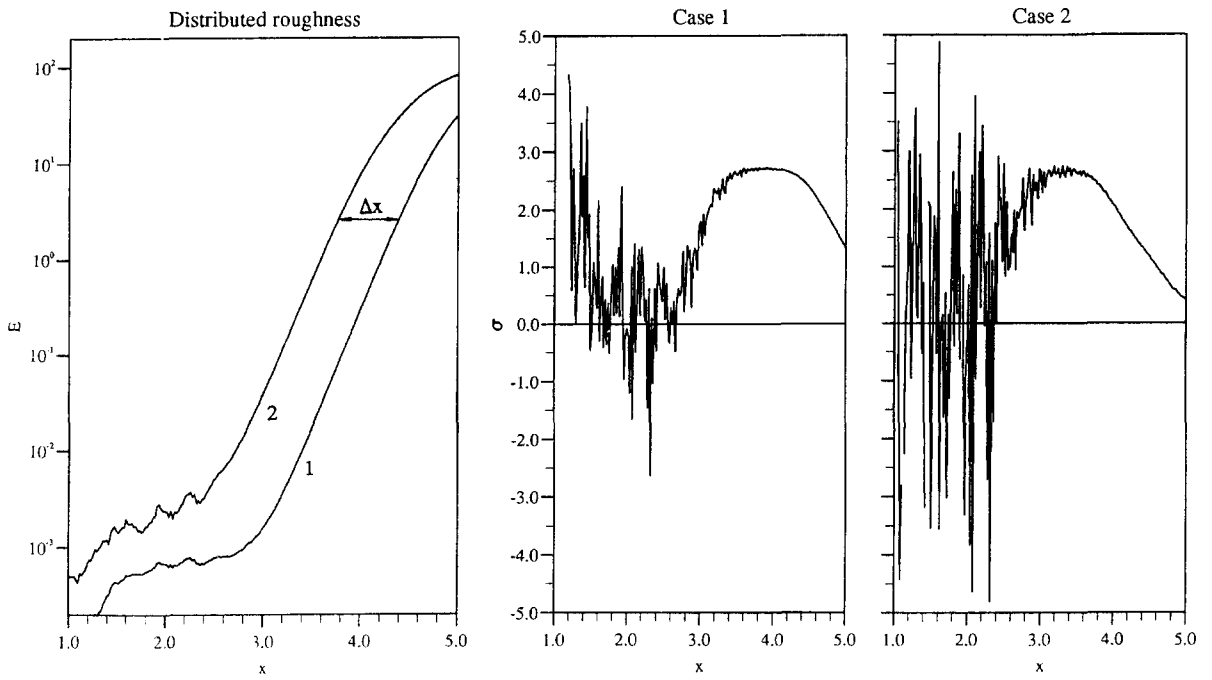

Fig. 2. Streamwise evolution of the perturbation energy E for the distributed roughness cases (left) and corresponding growth rates for cases 1 and 2.

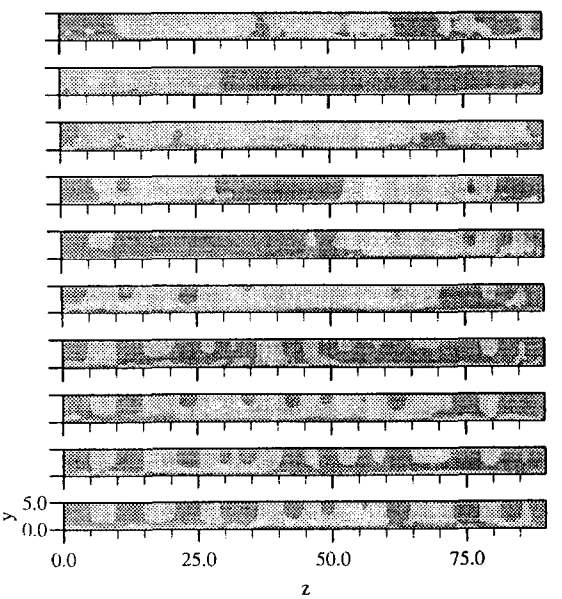

Fig. 3. Case 1: regions of positive (light shading) and negative (dark shading) streamwise vorticity for $x = 1.1 + 0.2i$, $i = 0, 1, \ldots, 9$, i increasing from top to bottom.

increasing x, there is a seemingly random coalescence of zones of equal sign vorticity; in the process, regions of opposite sign vorticity are engulfed or displaced. At each x the local field will be affected by (1) the upstream field and (2) the local forcing at the wall; the competition between these two mechanisms is the cause of the relatively long filtering length (x from 1 to about 2.7). The disturbance energy will start growing once a more or less regular alternation of positive and negative vorticity concentrations is created. These patches must be sufficiently organized and "strong" not to be affected any longer by the local wall forcing. Clearly, this is only a qualitative statement; in a linearized setting, a rigorous description of the causality relation between the solution at a given x and the history of the wall condition up to that x depends on a suitable kernel. Preliminary progress in this direction has been made by Luchini and Bottaro [22] who evaluated this kernel, a Green's function, via the solution of an adjoint system of parabolic partial differential equations with a reversed (backward) natural direction of evolution.

Back to the problem at hand, the reason why case 1 presents a slightly longer receptivity region when compared to case 2 is ascribed to the fact that the rough wall in 1 plays an active role on the flow field over a longer streamwise length. This is also the reason why the downstream flow evolution for the two cases differs somewhat, as can be inferred from Fig. 4, where isolines of the spanwise velocity on the plane $y = 0.9193$ are plotted. The $w = 0$ line is explicitly drawn to demonstrate the equivalence of the two cases for $x < 2.7$. Downstream of $x = 2.7$ differences start appearing because in case 1 the competing influences of upstream flow and wall forcing take place over a slightly longer streamwise distance. It is expected that differences will be more enhanced for larger roughness amplitude ratios. Differences in the receptivity lengths will cause different developments of the vortices.

As far as disturbance energy amplitudes are concerned, case 2 "preceds" case 1 of a distance $\Delta x \approx 0.6$, as shown on Fig. 2. Isolines of the velocity fields on two cross-sections of equal perturbation energies, $x = 5$ (case 1) and $x = 4.4$ (case 2) are plotted in Fig. 5. There are some similarities (stemming from the relatively long "common history") but also marked differences, e.g. a well-defined upwash zone is present at $z \approx 50$ in case 2 but not in case 1. Vortex pairs of different wavelengths and growth levels are present on the same cross-section; upright, symmetric vortices represent the exception in a world of deformed structures. The average wavelength Λ computed simply by counting the number of upwash regions (positive v at the wall) is equal to 233 for both cases, a value very close to that of the largest growth predicted by linear stability theory.

The preceding discussion suggests that a thin rough strip along z on an otherwise smooth plate should be more effective than random roughness in triggering Görtler vortices since the competition between upstream flow influence and local wall forcing occurs only over a reduced streamwise length, that of the strip. This case is discussed next.

4.2. *Cases 3–5: The rough strip*

Three cases are presented in this section and they are distinguished by the roughness function of the strip. In case 3, we have taken $g(x, z) = f_1(x, z)\exp[-50(x - 1.25)^2]$, in case 4 the rough strip is uniform along the span, $g(x, z) = f_2(x)\exp[-50(x - 1.25)^2]$, whereas in case 5 the wall presents a white noise distribution only in z : $g(x, z) = f_3(z)\exp[-50(x - 1.25)^2]$. The perturbation energies for cases 3–5 are plotted in Fig. 6. The presence of the strip is reflected in the relatively large increase in perturbation energies up to $x = 1.25$ and subsequent decrease downstream; for

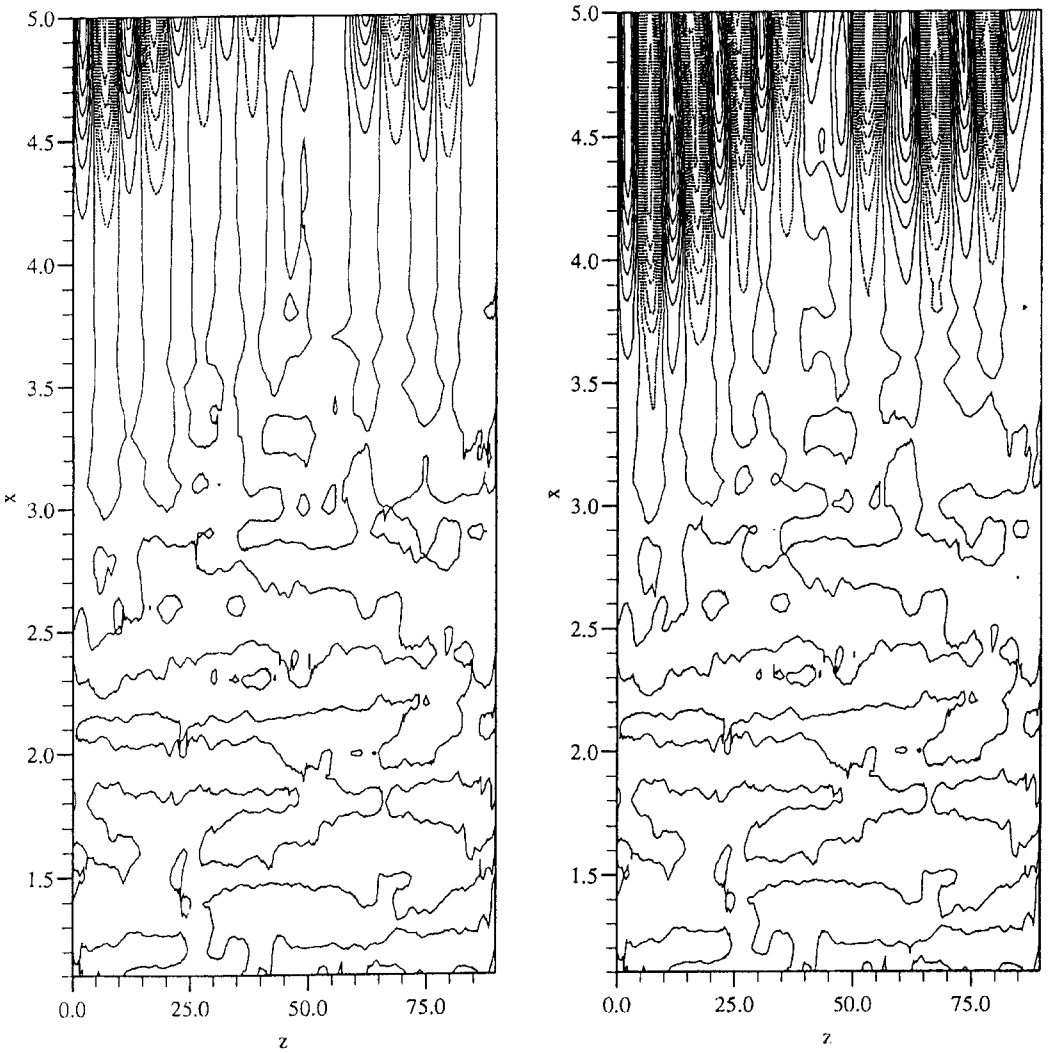

Fig. 4. Isolines of the spanwise velocity on the plane $y = 0.9193$ for case 1 (left) and case 2 (right). Isolines spacing is 1, negative values are shown with dotted lines.

$x > 1.7$ the three-configurations show marked differences. Growth rate curves (not shown) indicate that in case 3 the vortices start growing from $x \approx 2.0$; as expected a more rapid filtering is actuated when compared to cases 1 and 2, and the Gaussian strip is a better vortex promoter than distributed roughness. In case 4, where the roughness function depends only on x and streamwise vorticity cannot be created, the perturbation energy is exponentially damped for $x > 2.2$ and Görtler vortices do not form. Conversely, if the wall is grooved along x (case 5) the instability starts at $x \approx 1.7$. This is not unexpected since in this case the forcings from the upstream flow field and from the wall positively combine at all x's to enhance spanwise inhomogeneities.

Fig. 7 shows regions of negative and positive streamwise vorticity on different cross-sections $x = 1.1 + 0.1i$, $i = 0, 1, \ldots, 8$, for cases 3–5. Some non-zero streamwise vorticity is present in

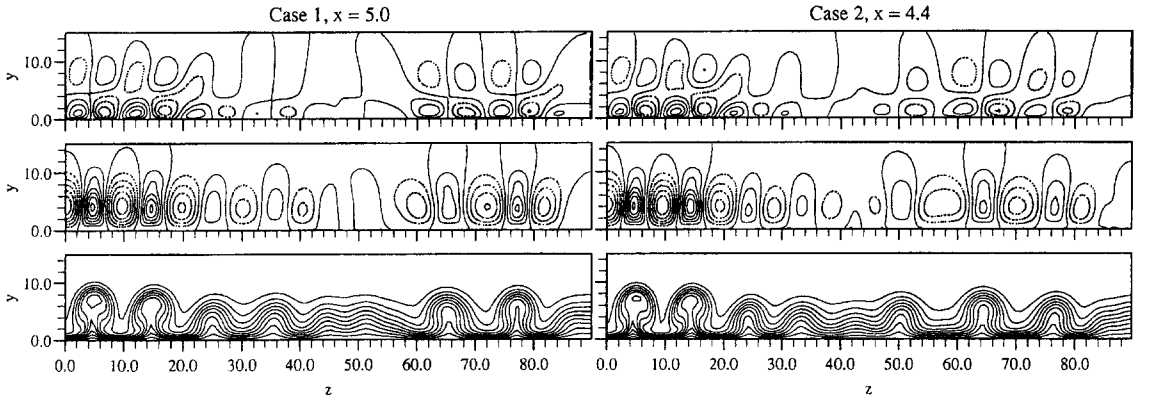

Fig. 5. Isolines of w, v and u (from top to bottom) for case 1 (left) and case 2 (right). Isolines spacing is 0.1 for the streamwise velocity component and 2 for the cross-stream components.

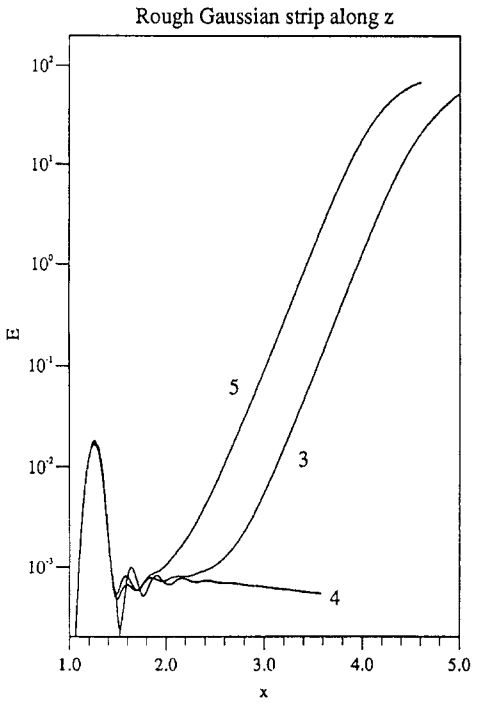

Fig. 6. Perturbation energy for the cases of the rough Gaussian strip centered on $x = 1.25$.

case 4, but it is solely due to computer round-off errors. The interesting cases are 3 and 5, and the difference between them is immediately apparent: the situation in 3 resembles that of the distributed roughness case, although here a regular alternation of well-defined patterns of vorticity concentration is formed faster since the wall is rough only over a relatively short streamwise distance. In case 5, one can easily follow the downstream evoluation of each negative or positive streamwise vorticity

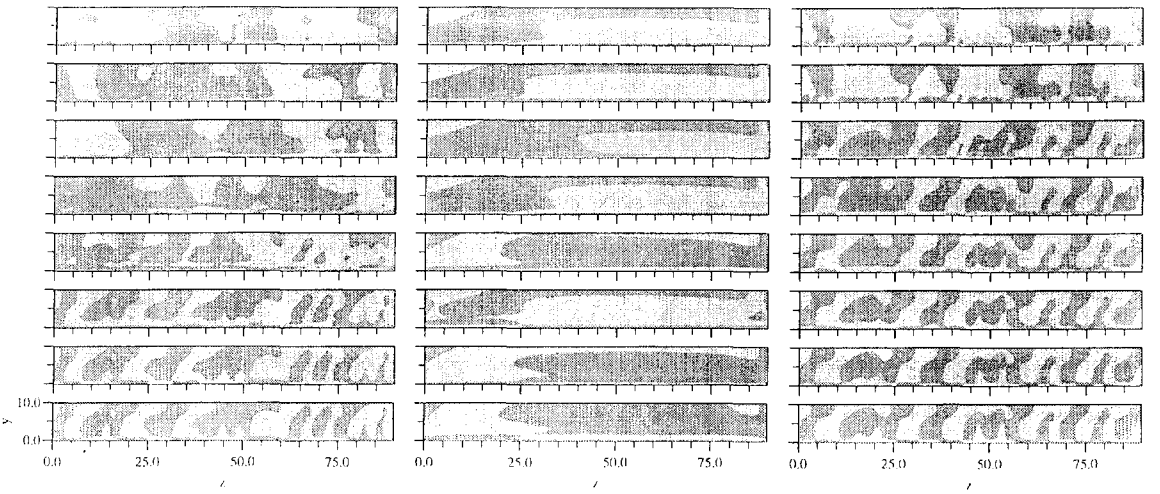

Fig. 7. Cases 3 (left); 4 (center) and 5: regions of positive (light shading) and negative (dark shading) streamwise vorticity for $x = 1.1 + 0.1i$, $i = 0, 1, \ldots, 8$, i increasing from top to bottom.

region, starting from the first station examined. This happens because, as already mentioned, forcings from the upstream flow and the rough wall do not counteract each other but act in a combined way. If vortex formation is the desired objective, case 5 indicates that a manner to promote it is to groove the wall along x, like in the case of riblets.

In Fig. 8 the streamwise velocity distribution on a z–x plane at $y = 0.9193$ is shown for cases 3 and 5. Average spanwise wavelengths in the two cases are, respectively, 255 and 233. The patterns of low- and high-speed streaks formed are reminiscent of those of turbulent boundary layers. Similarities between the two flow situations have been examined extensively by Blackwelder [23] and Bottaro et al. [6].

4.3. Case 6: Riblets

Triangular riblets of dimensionless wavelength s can be simulated by imposing the wall distribution as

$$g(x,z) = \left\{ \begin{array}{ll} \dfrac{2}{s}(z - ks) & \text{for } ks \leqslant z \leqslant (2k+1)s/2, \\ 2\left(1 - \dfrac{z - ks}{s}\right) & \text{for } (2k+1)s/2 \leqslant z \leqslant (k+1)s, \end{array} \right\} \quad k = 0, 1, 2, \ldots.$$

Three cases have been studied, corresponding to $s = 3.588$ (case 6.1, corresponding Görtler wavelength $\Lambda = 46$), $s = 9.966$ (case 6.2, $\Lambda = 212$) and $s = 22.425$ (case 6.3, $\Lambda = 717$). In the three configurations studied there is a brief initial transient phase until $x \approx 1.4$; downstream an exponential damping (case 6.1) or amplification (cases 6.2 and 6.3) of the disturbances occur (Fig. 9). The perturbations induced by the riblets have same wavelengths of the riblets, with downwash (secondary flow towards the wall) at the crests and upwash at the riblets valleys. Case 6.1 is not amplified, a fact consistent with both parallel and non-parallel local linear stability theories according to which

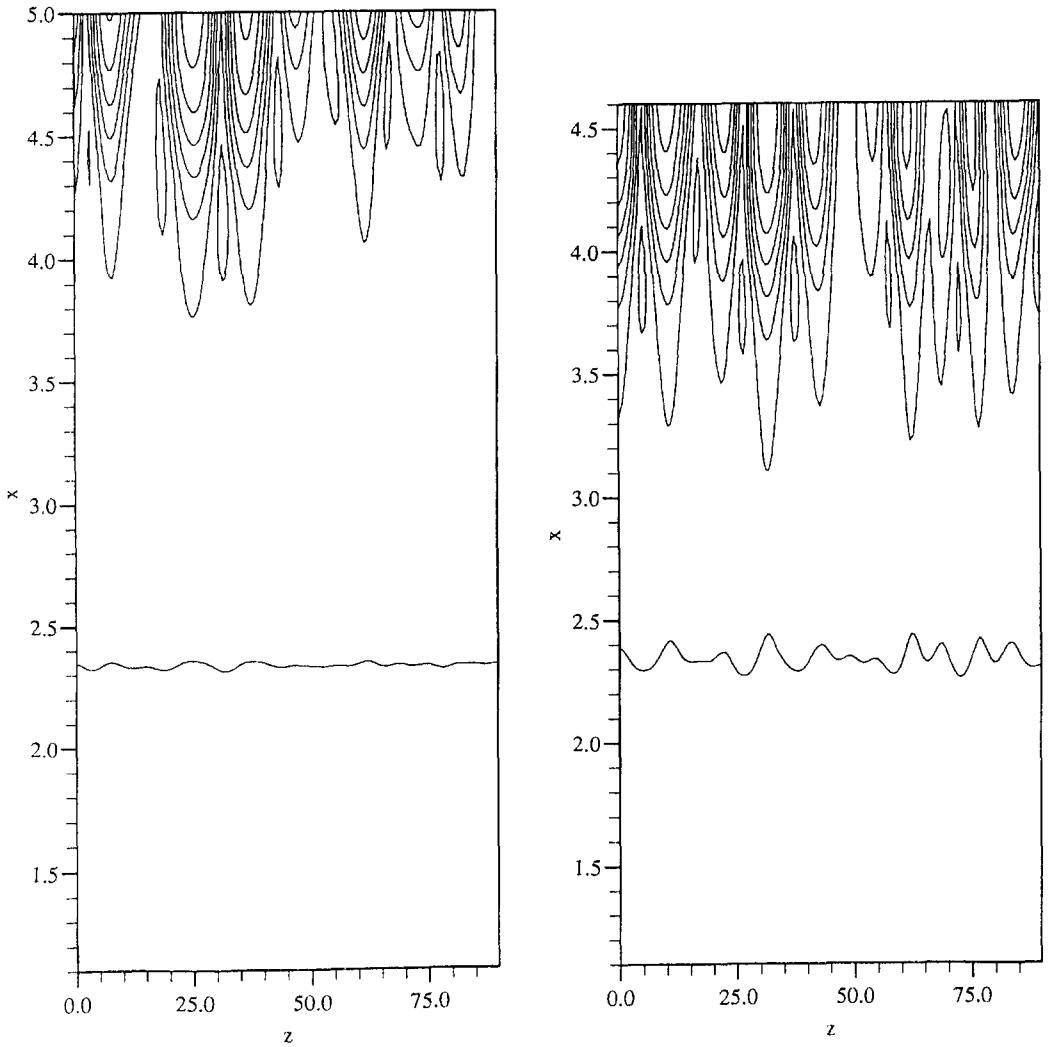

Fig. 8. Contours of the streamwise velocity for case 3 (left) and case 5 (right) on the plane $y = 0.9193$. Isoline spacing is 0.1.

perturbations are damped for all G when Λ is less than about 45. This decay in amplitude for the small wavelength limit case was also predicted by the analysis of Denier et al. [8]. Our calculation has, however, the surprising feature that the energy starts increasing after $x \approx 3.8$. This is due to the coalescence of equal sign vorticity regions on either side of $z = 65$, a coalescence made possible by minute losses of symmetry caused by round-off errors. During this process, exemplified in Fig. 10, a coherent structure of larger wavelength is formed. It is this new structure that can be amplified and that produces the increase of the disturbance energy. It is to be noted that this event would always occur in an experimental facility equipped with small-wavelength riblets, because of the inevitable manufacturing imperfections of the riblets. Note also that this merging of equal sign vorticity regions differs from the 3 to 2 merging event of non-linear streamwise vortices caused by a generalized Eckhaus instability described by Bottaro [24] and Guo and Finlay [25].

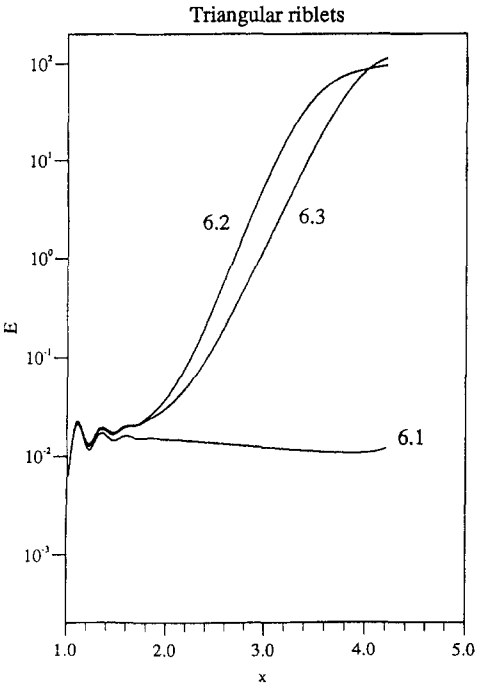

Fig. 9. Disturbance energy versus x for triangular riblets of different spanwise wavelengths.

In cases 6.2 and 6.3 regular arrays of Görtler vortices are formed, as shown in Fig. 11. The rapid growth of the disturbance energy in these cases is in agreement with the analysis of Bassom and Hall [9] for the situation of distributed wall forcing of spanwise wavelength of the order of the boundary layer thickness. For $\Lambda = 212$ a larger growth rate is found as by linear stability theory [5, 6]; interestingly, the total integrated perturbation energy at saturation is bigger for the larger wavelength case.

4.4. *Case 7: The three-dimensional hump*

The last case studied is that of an isolated three-dimensional hump centered at $x = 1.25$ and $z = 35$, with wall function prescribed by $g(x,z) = \exp[-50(x-1.25)^2]\exp[-(z-35)^2]$. Bassom and Hall [9] considered an isolated element consisting of a delta function-shaped wall forcing – a necessary assumption to make analytical progress – and concluded that isolated roughness is inefficient in generating Görtler vortices. For the more realistic wall forcing treated here quasi-exponential growth is found immediately downstream of the hump, as shown in Fig. 12. Two regions appear, with different growth rates: An initial one, up to $x \approx 2$, of slow amplification, and a second one for $x > 2.2$ with same growth rate as that of a vortex with $\Lambda \approx 210$. The initial perturbation produced by the hump is uniformly spread over a large z range; around $x \approx 2$ an area of concentrated disturbances emerges. Further downstream a high-speed streak is produced along x at $z = 35$, with two vortex pairs symmetric about $z = 35$; the rest of the cross-section seems unaffected by the presence of the roughness element (Fig. 13). Clearly, if the height of the element had exceeded some critical

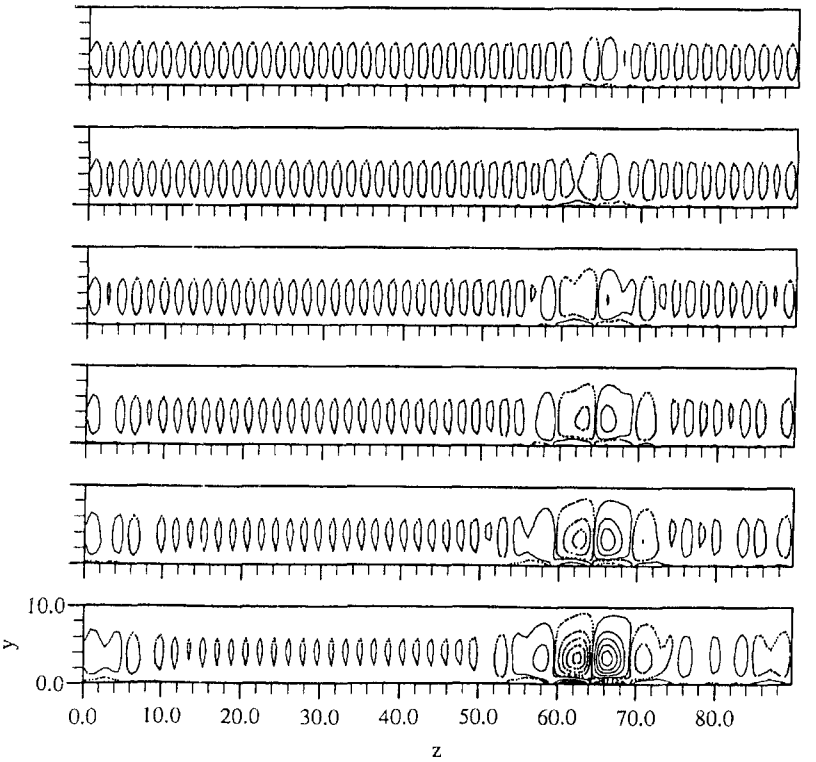

Fig. 10. Case 6.1. Development of the streamwise vorticity for, from the top, $x = 3.2 + 0.2i$, $i = 0, 1, \ldots, 5$. The coalescence of regions of equal sign vorticity on either sides of $z = 65$ (and consequent annihilations of zones of opposite sign vorticity contained in between the two merging regions) is clearly visible starting from $x = 3.6$; this localized process has repercussions downstream and further mergings are under way. The minimum absolute value of the isolines shown is 0.05, spacing between adjacent lines is 0.03 and negative contours are plotted with dotted lines.

value, boundary layer separation would have occurred with consequent rapid transition to turbulence. To deal with such an event interacting boundary layer theory [26], triple-deck theory [27] or full Navier–Stokes computations are needed.

5. Concluding remarks

This paper presents the first numerical experiments of linearly and non-linearly spatially developing Görtler vortices promoted uniquely by small-amplitude surface roughness; unlike Bertolotti's work [10], no perturbation is superposed to the basic Blasius flow at the inflow of our computational domain. Several surfaces not previously examined have been treated here and their effect as near-wall vortex "generators" elucidated. This was made possible because our parabolic model was found to accurately describe the physics, as proven in the Appendix.

Our results demonstrate that ribleted surfaces of sufficiently large spanwise wavelength are extremely efficient in triggering Görtler vortices of that particular wavelength, whereas very small-wavelength riblets (Λ less than about 50) or grooves cut along the spanwise direction do not promote

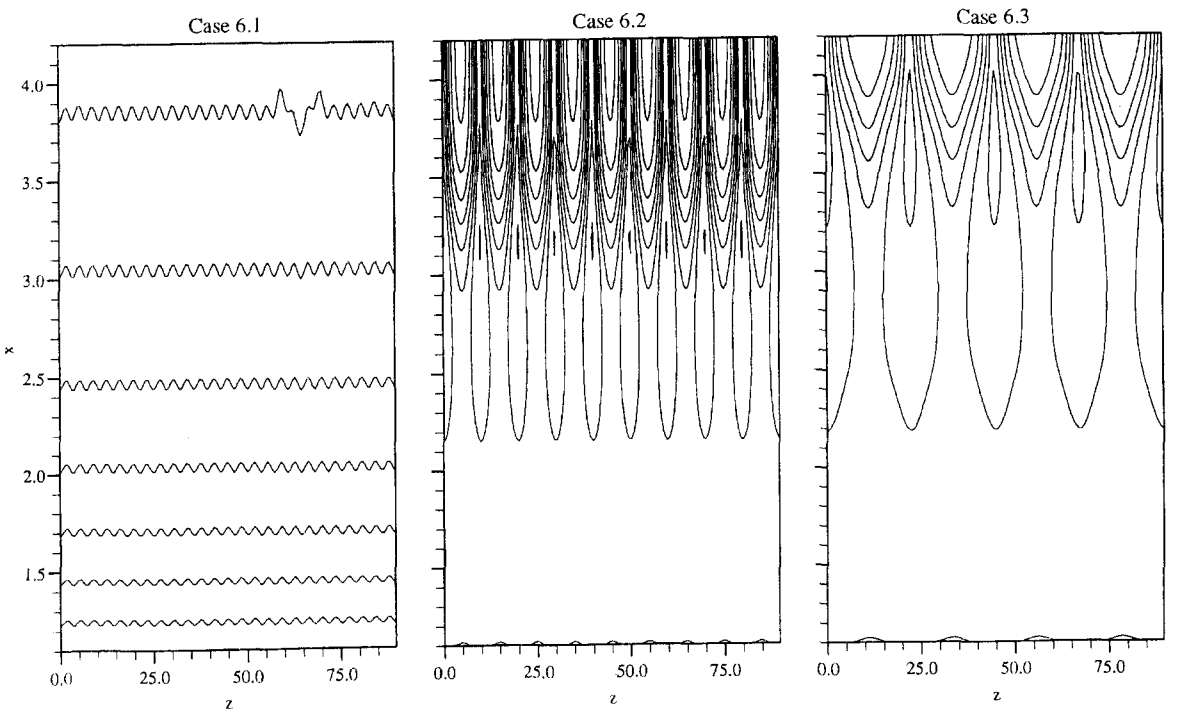

Fig. 11. Streamwise velocity isolines on the $y = 0.9193$ plane for the ribleted walls. For case 6.1 isoline values range from 0.16 to 0.3 with interval of 0.02; for case 6.2 the contours go from 0.1 to 0.8 with 0.1 spacing and for case 6.3 the values range from 0.1 to 0.7 with 0.1 spacing.

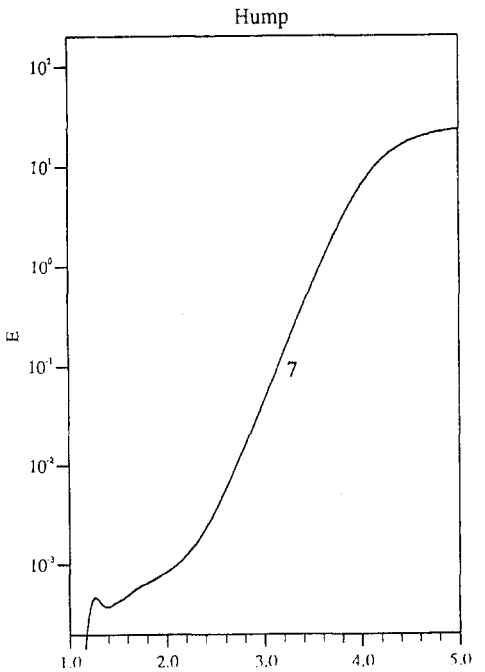

Fig. 12. Downstream development of the perturbation energy for the hump.

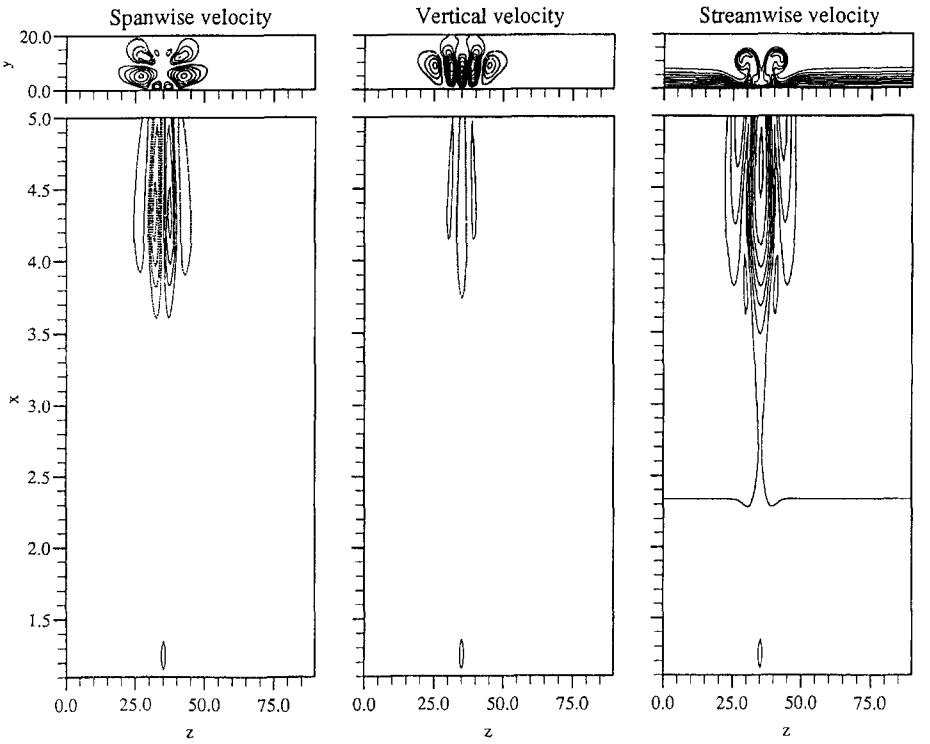

Fig. 13. Isolines of the velocity components for the isolated hump. Contours are shown both on the cross-section $x = 5$ (top figures) and on the spanwise–streamwise plane $y = 0.9193$. Isolines spacings are 0.1 for u and 2 for v and w. Positive values are shown with solid lines, zero lines are omitted. The position and shape of the hump are represented on the three bottom figures via the contour $\varepsilon g(x,z) = 0.03$.

the vortex development. For all cases examined there is a linear filtering (receptivity) region before the instability can start amplifying disturbances. The streamwise length of such region depends on wall type and roughness amplitude. A boundary layer tripped over a short streamwise distance by a thin strip reacts more rapidly (appropriate perturbations develop faster and can be exponentially amplified earlier) than one uniformly perturbed at the wall. When isolated roughness elements are employed, the disturbance energy increases immediately but the vortices remain localized. Under a broad-band distribution of spanwise roughness wavenumbers it is found that Görtler vortices of average wavelength close to that of largest growth of the linear stability theory develop.

One interesting question brought about by the present study is whether small-wavelength riblets or spanwise grooves can act to suppress or delay the growth of Görtler vortices induced, for example, by free-stream turbulence. Some effect on the vortices would not be unexpected for the case of a wall equipped with riblets of spanwise scale smaller than that of the streaks, simply by analogy to the case of turbulent boundary layers. This issue awaits further investigations.

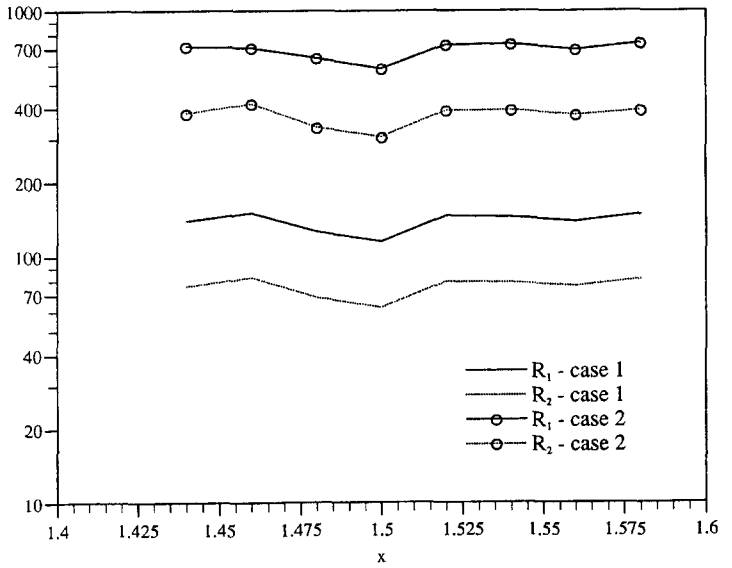

Fig. 14. "Ellipticity factors" R_1 and R_2 versus x for cases 1 and 2.

Acknowledgements

A.B. acknowledges support from the Swiss National Fund, grant number 21-36035.92; A.Z.'s visit to EPFL was made possible by an ERCOFTAC visitor grant. Computing time on the Cray Y-MP was generously provided by the EPFL Service Informatique Centrale. Prof. P.A. Monkewitz and Dr. K. Roussopoulos are acknowledged for interesting discussions.

Appendix. An a posteriori justification for the parabolic approach

The parabolic Eqs. (4)–(7) were derived to investigate the spatial development of Görtler vortices over smooth walls (see e.g. Ref. [12]). The underlying assumption is that of slow streamwise variation, so that streamwise diffusion terms can be labelled as negligible when compared to cross-stream diffusion terms. Because the wall boundary condition here is, in general, not a slow function of x, it has to be verified a posteriori that the solution presents slowly varying properties in the streamwise direction. For, if this is not the case, the elliptic effects of these rapid variations would be important and could not be ignored.

The most offending situations are cases 1 and 2, in the initial receptivity region as evidenced by Fig. 2. For our check we have monitored, for x in the range $1.4 < x < 1.6$, the streamwise development of the extrema of $\partial^2 u/\partial x^2$, $\partial^2 u/\partial y^2$ and $u\partial u/\partial x$. We call R_1 the ratio of the first to the second, and R_2 the ratio of the first to the third; R_1 and R_2 are measures of the ellipticity of the system and are plotted in Fig. 14. In case 2 ($\varepsilon = 0.025$) R_1 and R_2 are of the order of 500, whereas in case 1 ($\varepsilon = 0.005$) they are of the order of 100. Since, from the scalings proposed in Eqs. (2) and (3), terms like $\partial^2 u/\partial x^2$ are multiplied by Re^{-1} (here taken to be 7.5×10^{-6}) and hence discarded as asymptotically small, we conclude that the parabolic approximation is tenable for the cases at hand.

It would not be tenable if R_1 and R_2 were of order Re. As expected (and confirmed by Fig. 14) the quality of the parabolic solutions degrades as the roughness amplitude is increased.

References

[1] I. Tani, Prediction of longitudinal vortices in the boundary layer along a curved wall, J. Geophys. Res. 67 (1962) 3075.

[2] H. Bippes and H. Görtler, Dreidimensionale Störungen in der Grenzschicht an einer konkaven Wand, Acta Mechanica 14 (1972) 251.

[3] J.D. Swearingen and R.F. Blackwelder, The growth and breakdown of streamwise vortices in the presence of a wall, J. Fluid Mech. 182 (1987) 255.

[4] P. Petitjeans, Étude expérimentale des instabilités de couche limites sur des parois concaves: instabilité de Görtler, Ph.D. Thesis, University Paris VI (1992).

[5] J.M. Floryan and W.S. Saric, Stability of Görtler vortices in boundary layers, AIAA J. 20 (1982) 316; see also: Wavelength selection and the growth of Görtler vortices, AIAA J. 22 (1984) 1529.

[6] A. Bottaro, B.G.B. Klingmann and A. Zebib, Görtler vortices with system rotation, Theoret. Comput. Fluid Dyn. 8 (1996) 325.

[7] P. Hall, Görtler vortices in growing boundary-layers: the leading edge receptivity problem, linear growth and the non-linear breakdown stage, Mathematika 37 (1990) 151.

[8] J.P. Denier, P. Hall and S. Seddougui, On the receptivity problem for Görtler vortices: vortex motions induced by wall roughness, Phil. Trans. Roy. Soc. London A 335 (1991) 51.

[9] A.P. Bassom and P. Hall, On the receptivity problem for O(1) wavelength Görtler vortices, Proc. Roy. Soc. A 446 (1994) 499.

[10] F.P. Bertolotti, Vortex generation and wave-vortex interaction over a concave plate with roughness and suction, ICASE Report No. 93-101.

[11] J.D. Swearingen and R.F. Blackwelder, Parameters controlling the spacing of streamwise vortices on concave walls, AIAA Paper No. 83-0380 (1983).

[12] P. Hall, The linear development of Görtler vortices in growing boundary layers, J. Fluid Mech. 130 (1983) 41.

[13] H. Bippes and H. Deyhle, Das receptivity-problem in Grenzschichten mit längswirbelartigen Störungen, Z. Flugwiss. Weltraumforsch. 16 (1992) 34.

[14] B. Müller and H. Bippes, Experimental study of instability modes in a three-dimensional boundary layer, in: Fluid Dynamics of Three-Dimensional Turbulent Shear Flows and Transition, AGARD C-P 438 (1988).

[15] H. Bippes and B. Müller, Disturbance growth in an unstable three-dimensional boundary layer, in: Numerical and Physical Aspects of Aerodynamic Flows, Vol. IV, ed. T. Cebeci (Springer, Berlin, 1990).

[16] H. Bippes, Experiments on transition in three-dimensional accelerated boundary layer flows, in: Proc. R.Ae.S. Boundary Layer Transition and Control (Cambridge, UK, 1991).

[17] R.H. Radeztsky Jr., M.S. Reibert, W.S. Saric and S. Takagi, Effect of micronsized roughness on transition in swept-wing flows, AIAA Paper No. 93-0076 (1993).

[18] R.H. Radeztsky Jr., M.S. Reibert and W.S. Saric, Development of stationary cross-flow vortices on a swept wing, AIAA Paper No. 94-2373 (1994).

[19] W.S. Saric, J.A. Hoos and R.H. Radeztsky Jr., Boundary layer receptivity of sound with roughness, in: Boundary Layer Stability and Transition, ASME FED, Vol. 114, eds. D.C. Reda, H.L. Reed and R. Kobayashi (1991).

[20] P.R. Spalart, Numerical study of transition induced by suction devices, in: Near-wall Turbulent Flows, eds: R.M.C. So, C.G. Speziale and B.E. Launder (Elsevier, Amsterdam, 1993) p. 849.

[21] S.V. Patankar and D.B. Spalding, A calculation procedure for heat, mass and momentum transfer in three-dimensional parabolic flows, Int. J. Heat Mass Transfer 15 (1972) 1787.

[22] P. Luchini and A. Bottaro, A time-reversed approach to the study of Görtler instabilities, in: Advances in Turbulence VI, eds. S. Gantilakis, L. Machiels and P.A. Monkewitz (Kluwer Academic Publishers, Dordrecht, 1996) p. 369.

[23] R.F. Blackwelder, Analogies between transitional and turbulent boundary layers, Phys. Fluids 26 (1983) 2807.

[24] A. Bottaro, On longitudinal vortices in curved channel flow, J. Fluid Mech. 251 (1993) 627.
[25] Y. Guo and W.H. Finlay, Wavenumber selection and irregularity of spatially developing non-linear Dean and Görtler vortices, J. Fluid Mech. 264 (1994) 1.
[26] R.T. Davis, A procedure for solving the compressible interacting boundary layer equations for subsonic and supersonic flows, AIAA paper 84-1614 (1984).
[27] F.T. Smith and J.H. Merkin, Triple-deck solutions for subsonic flow past humps, steps, concave or convex corners and wedge trailing edges, J. Comp. Phys. 10 (1982) 7.